

Observation of interface induced high temperature superconductivity in single unit-cell FeSe films on SrTiO₃(110)

Guanyu Zhou¹, Ding Zhang¹, Chong Liu¹, Chenjia Tang¹, Xiaoxiao Wang¹, Zheng Li¹,
Canli Song^{1,2}, Shuaihua Ji^{1,2}, Ke He^{1,2}, Lili Wang^{1,2*}, Xucun Ma^{1,2} and Qi-Kun Xue^{1,2†}

¹ *State Key Laboratory of Low-Dimensional Quantum Physics, Department of Physics, Tsinghua University, Beijing 100084, China*

² *Collaborative Innovation Center of Quantum Matter, Beijing 100084, China*

We report high temperature superconductivity in one unit-cell (1-UC) FeSe films grown on STO(110) substrate by molecular beam epitaxy (MBE). By *in-situ* scanning tunneling spectroscopy measurement, we observed a superconducting gap as large as 17 meV. Transport measurements on 1-UC FeSe/STO(110) capped with FeTe layers reveal superconductivity with an onset T_C of 31.6 K and an upper critical magnetic field of 30.2 T. We also find that the T_C can be further increased by an external electric field, but the effect is smaller than that on STO(001) substrate. The study points out the important roles of interface related charge transfer and electron-phonon coupling in the high temperature superconductivity of FeSe/STO.

The single unit cell (UC) films of FeSe on perovskite SrTiO₃(STO)(001) substrate (referred as FeSe/STO(001) hereafter) exhibits probably the highest superconducting transition temperature T_C [1] among all the heterostructure systems discovered so far. A superconducting gap of 20 meV[1], almost one order of magnitude larger than that of bulk FeSe[2], was observed by scanning tunneling microscopy (STM). Angle resolved photoemission spectroscopy (ARPES) revealed a similar gap that closed at ~65 K[3-5], while transport measurement on this system covered by FeTe capping layers demonstrated a superconducting transition temperature $T_C > 40$ K[6]. *Ex situ* mutual inductance and *in situ* four-probe measurements even indicated a transition temperature of 65 K[7] and 100 K[8], respectively, which were even higher than the record $T_C = 55$ K of bulk iron-based superconductors[9].

The advent of enhanced superconductivity in FeSe/STO(001) has instigated great interests in other interfacial systems[10] both experimentally [11-15] and theoretically[1, 16, 17]. For example, by replacing FeSe with FeTe_{1-x}Se_x a superconducting gap of 17 meV was observed[13], while using BaTiO₃ and strained STO substrates led to a gap closing temperature up to 75 K[11, 12]. The investigations reveal the crucial roles of interface charge transfer[3-5, 16, 18] and electron-phonon coupling[1, 15-17] in boosting the superconductivity. In addition, stress caused by lattice mismatch between FeSe and STO substrate is also thought to be responsible for T_C enhancement[4]. To figure out the key role of substrate, STO(110) substrate is of great interest because it resembles STO(001) in high density subsurface oxygen vacancies[19, 20] but distinguishes itself by anisotropic in-plane lattice constants[19] and dielectric constant[21]. Here, we investigated molecular beam epitaxy (MBE) growth of 1-UC FeSe films on STO(110) substrates (referred as FeSe/STO(110) hereafter) and studied the superconducting properties by combined *in-situ* STS and *ex-situ* transport measurement.

One UC FeSe in β -phase consists of two Se layers sandwiching a Fe layer with in-plane lattice constant of 3.78 Å and out-of-plane lattice constant of 5.50 Å[22]. STO, the archetypical perovskite oxide, has a lattice constant of 3.91 Å[23]. Along the [110] direction, it is composed of alternating SrTiO⁴⁺ and O₂⁴⁻ layers and hence polar. For charge compensation, the top surface transforms into a tetrahedrally coordinated titania layer [19, 24] reconstructed with $n \times 1$ periodicities ($n=2, 3, 4, 5, 6 \dots$ corresponds to the reconstruction along the [001] direction.)[23]. Here, the Nb-STO(110) substrate exhibits uniform 4×1 surface reconstruction (Fig. S1)[25].

Figs. 1(a)-(b) display the typical atomic-resolution STM topographic images of 1-UC FeSe films epitaxial grown on the Nb-STO(110)-(4×1) substrate in which each bright spot corresponds to a surface Se atom in a Se-Fe-Se triple layer. The 1-UC FeSe films ripple (Fig. 1(a)) and exhibit strong local distortion (Fig. 1(b)). Fourier transformation of Fig. 1(a) gives nearly consistent lattice constants of 3.88 and 3.87 Å along the two orthogonal directions, whereas, a statistical analysis of atom-atom separations as shown in Fig. 1(b) demonstrates anisotropic lattice constants of 3.87 ± 1.0 Å and 3.79 ± 1.1 Å along the [001] and [1-10] directions of STO, respectively. A representative dI/dV spectrum taken on the 1-UC FeSe films at 4.6 K exhibits a gap of 17 meV, defined by half the distance between two coherence peaks (Fig.1(e)), similar in magnitude to most reports of the superconducting gaps[3-5] but slightly smaller than the maximum value (20 meV) in FeSe/STO(001)[1] .

To establish that the gap opening as observed in Fig. 1(e) corresponds to superconducting transition, we performed *ex situ* transport measurements. Here we use insulating STO substrates. 1-UC FeSe is capped by 10-UC FeTe layer which is insulating and has been successfully used to protect FeSe/STO(001) from ambient contamination/oxidation[6]. The morphology of the FeSe films follows the terrace-step structure of STO(110) substrate, as evidenced by a step height of 2.7 Å (Fig. S2) which is equal to the out-of-plane lattice constant of STO along [110] direction[23], indicating a perfect layer-by-layer growth. Figs. 1(c)-(d) display typical atomically resolved STM topographic images of 1-UC FeSe films on insulating STO(110) substrate. In contrast to rippled films observed on Nb-STO substrate, the 1-UC FeSe films on insulating STO exhibit nearly ordered stripe patterns with a period of 2.34 ± 0.03 nm (Fig. 1(c) and Fig. S2). Moreover, the lattice constants are distinctly anisotropic, 3.89 Å (3.93 ± 0.5 Å) and 3.75 Å (3.78 ± 0.6 Å) along the [001] and [1-10] directions of STO as revealed by Fourier transformation shown in Fig. 1(c) (local distortion in Fig. 1(d)), respectively. It suggests that the 1-UC FeSe films are ~3% expanded and ~1% contracted in the two orthogonal directions. The lattice mismatch resulted strain may be partially released as the Fe/Se atoms shift their vertical positions in the STO-[110] direction, which is evidenced by the observed rippled (striped) modulation in FeSe films on Nb-STO (insulating STO) substrate. The contrast in the modulation, i.e. ripple vs. stripe, could be due to the temperature dependent reconstruction of STO(110) surface[23, 25]. The local lattice distortion in the striped FeSe films (± 0.5 Å) (Fig.

1 (c)) is half that in rippled FeSe films ($\pm 1.0 \text{ \AA}$) (Fig. 1(a)). The 4% anisotropy is therefore clearly resolved in the former case. Based on the above observation, we proposed a model to show the epitaxial relation between FeSe films and STO(110) substrate. As depicted in Fig. 1(g), along the [1-10] direction of STO, three unit cells of FeSe coincide with two unit cells of STO, whereas an one-to-one correspondence between FeSe and STO exists along the [001] direction.

Figure 2(a) displays the sample resistance as a function of temperature at zero field (a schematic setup for transport measurement is shown in the inset). The resistance exhibits a linear dependence on temperature below 100 K, deviates from linearity at 47 K, and drops by three orders of magnitude till 16 K. By extrapolating the normal resistance and the superconducting transition curves, we obtain an onset temperature of $T_{onset} \sim 31.6 \text{ K}$, which is almost four times of the $T_C \sim 8 \text{ K}$ for bulk FeSe[22]. The inset in Fig. 2(b) shows the resistance as a function of temperature at various magnetic fields applied perpendicular to the film. We can clearly see that as the magnetic field increases, the superconductivity transition region becomes broader and T_C shifts to lower temperatures. For a 2D superconductor, its response to an external magnetic field normal to the 2D plane is expected to follow the linear Ginzburg-Landau formula[26]:

$$\mu_0 H_{C2} = \frac{\Phi_0}{2\pi\xi^2} \left(1 - \frac{T_c}{T_{c,H_{C2}(0)}}\right) \quad (1),$$

here $\mu_0 H_{C2}$ is the upper critical field, ξ the in-plane coherent length, and $\Phi_0 = h/2e$ the flux quantum. $T_{c,H_{C2}(0)}$ and T_C represent the superconducting transition temperature at zero field and finite fields, respectively. Due to the 2D nature of this system, the superconducting transition spreads in a broad temperature window of more than 10 K. Here, we use the mid-point temperature T_{mid} at which the resistance drops to 50% of the normal state resistance, namely $R(T_{mid}) = 50\% R_{norm}$ to estimate the upper critical field. As shown in Fig. 2(b), T_{mid} indeed behave linearly with the magnetic field up to 9 T, consistent with the formula (1). The linear fitting gives an upper critical field of $\mu_0 H_{C2(110)} \sim 30.2 \text{ T}$. The coherent length calculated by using Eq. (1) is $\xi_{(110)} = 3.3 \text{ nm}$. These values are much larger than the thickness of single UC FeSe (0.55nm), attesting to its 2D superconductivity nature. In the case of FeSe/STO(001)[6], the upper critical field is 56.8 T and the coherent length $\xi_{(001)} = 2.4 \text{ nm}$ (Fig. 2(b)). From the

BCS theory[27], the relation $\xi_{(110)} > \xi_{(001)}$ implies that the superconducting gap in FeSe/STO(110) system should be smaller than that in FeSe/STO(001). It is consistent with the results that $\Delta_{(110)} \sim 17 \text{ meV} < \Delta_{(001)} \sim 20 \text{ meV}$ [1] and $T_{onset(110)} \sim 31.6 \text{ K} < T_{onset(001)} \sim 40.2 \text{ K}$ [6].

The 2D superconductivity is evidenced by the signature of Berezinski–Kosterlitz–Thouless (BKT) transition[28]. The $V(I)$ characteristics shown in Fig. 3(a) was measured at temperatures ranging from 16 to 45 K at zero field. The $V(I)$ curves exhibit a $V \sim I^\alpha$ power-law dependence, and the slope corresponding to the exponent changes systematically as expected for the BKT transition[28, 29]. A detailed evolution of the α -exponent as a function of temperature is summarized in Fig. 3(b). With decreasing temperature, the exponent α deviates from 1 and approaches 3 at 24 K, the temperature identified as T_{BKT} . Additionally, the observed $R(T)$ characteristics are consistent with a BKT transition. Just above T_{BKT} , the resistance has the following temperature dependence: $R(T) = R_0 \exp[-b(T/T_{BKT} - 1)^{-1/2}]$, where R_0 and b are material parameters[30]. Plotting $[d\ln(R)/dT]^{-2/3}$ against T would therefore reveal a linear dependence with the extrapolation of $[d\ln(R)/dT]^{-2/3}$ to zero at T_{BKT} . As shown in Fig. 3(c), such an extrapolation yields $T_{BKT} = 24.1 \text{ K}$, which is in agreement with the result of the $V-I^\alpha$ analysis.

Similar to FeSe/STO(001), FeSe/STO(110) is a superconductor dominated by n-type carriers[31]. The Hall coefficient exhibits the same evolution with decreasing temperature[31], *i.e.* changing from positive to negative values at a temperature around 120-130 K before the superconducting transition and then remaining at negative values (inset of Fig.4(a)). Using STO as a back gate is expected to electrostatically modulate the superconductivity. Fig. 4(a) displays the resistance as a function of temperature at various gate voltages (V_g) for FeSe/STO(110). Under negative bias, the superconducting transition shifts steadily to lower temperatures and T_{onset} decreases by 2.8 K at a voltage of -200 V. On the other hand, a much weaker enhancement of 0.5 K is present under positive gating, which may reflect that an optimal doping is nearly approached. Such a dichotomy was previously observed in the FeSe/STO(001) system[31], which is re-plotted in Fig. 4(b). Fig. 4(c) shows a comparison between FeSe/STO(110) and FeSe/STO(001), where the superconducting transition temperature T_{onset} is plotted as a function of gate voltage V_g . Clearly, the modulation of superconductivity with electrostatic gating is smaller for FeSe/STO(110) interface than for FeSe/STO(001) interface.

The above results suggests a smaller interface enhancing factor for FeSe/STO(110) than for FeSe/STO(001), as FeSe/STO(110) exhibits a comparable but smaller superconducting gap, lower T_C and weaker modulation under same gate voltages. This comparison provides us with some insights into the key factors/effects of the interface high temperature superconductivity. From the structure point of view, FeSe/STO(110) exhibits 1% contraction and 3% expansion along the two orthogonal directions relative to bulk FeSe, strikingly differing from FeSe/STO(001) where 3% expansion is observed for both directions [15]. Nevertheless, the superconducting gap observed here (17 meV) is comparable with the gap in FeSe/STO(001) within experimental uncertainty[3-5] or merely ~15% off the optimal value[1]. Strain can be therefore excluded from the critical factors for the interface high temperature superconductivity in FeSe/STO. The lattice variation would significantly affect the antiferromagnetic superexchange interactions between Fe moments[32]. Its minor role speaks against that antiferromagnetic-interaction/spin-fluctuation is responsible for electron pairing here. Rather, the remarkably enhanced superconductivity with comparable superconducting gaps in both FeSe/STO(110) and FeSe/STO(001) favors the scenario of interface enhanced electron-phonon coupling [16, 17]. Both systems host similar 2D carrier densities (due to oxygen vacancies)[19, 20], and O-Ti-O stretching modes with energy at ~ 100 meV[33, 34], which couples with FeSe electrons and contributes to superconductivity as revealed by ARPES study[16]. Furthermore, according to the theoretical picture in Ref. 17, the interface electron-phonon coupling constant is proportional to $\sqrt{\epsilon_{\parallel}/\epsilon_{\perp}}$, where ϵ_{\parallel} and ϵ_{\perp} are the dielectric constants parallel and perpendicular to the FeSe/STO interface, respectively. Meanwhile, for the 2D superconductivity where the electrons are confined in the plane parallel to the FeSe/STO interface, in-plane dielectric constant ϵ_{\parallel} is the control factor of electron screening and Coulomb interaction. Hence, the fact that ϵ_{\parallel} (ϵ_{\perp}) of FeSe/STO(110) is smaller (larger) than that of FeSe/STO(001) ($\epsilon_{[001]} < \epsilon_{[1-10]} < \epsilon_{[100]} < \epsilon_{[110]}$)[21] should result in lower T_C in FeSe/STO(110), which is consistent with our experimental results. It is worth noting that the weaker modulation of superconductivity by electrostatic gating and lower upper critical field for FeSe/STO(110) interface could be due to larger spatial extension of 2D carriers along [110]

direction [26]. This implies that stronger confinement of 2D carriers promotes higher T_C , which is also consistent with the idea of interface superconductivity.

In conclusion, we demonstrate the interface enhanced superconductivity in 1-UC FeSe films on STO(110) by *in situ* STS and direct transport study. By comparing with FeSe/STO(001) systems, we show that the electron-phonon coupling proposed in our previous study [1] plays very crucial role in the high T_C superconductivity in 1-UC FeSe films on STO substrates. This work demonstrates an explicit and feasible way for rational design and preparation of high T_c superconductors by interface engineering.

This work is supported by NSFC (91421312, 91121004, 11574174 and 11404183) and MOST of China (2015CB921000).

G.Y. Zhou, D. Zhang and C. Liu contributed equally to this work.

*liliwang@mail.tsinghua.edu.cn

†gkxue@mail.tsinghua.edu.cn

- [1] Q.-Y. Wang *et al.*, Chin. Phys. Lett. **29**, 037402 (2012).
- [2] C.-L. Song *et al.*, Science **332**, 1410 (2011).
- [3] D. Liu *et al.*, Nat. Commun. **3**, 931 (2012).
- [4] S. Tan *et al.*, Nat. Mater. **12**, 634 (2013).
- [5] S. He *et al.*, Nat. Mater. **12**, 605 (2013).
- [6] W.-H. Zhang *et al.*, Chin. Phys. Lett. **31**, 017401 (2014).
- [7] Z. Zhang *et al.*, Sci. Bull. **60**, 1301 (2015).
- [8] J. F. Ge *et al.*, Nat. Mater. **14**, 285 (2015).
- [9] Z. Ren *et al.*, Chin. Phys. Lett. **25**, 2215 (2008).
- [10] I. Bozovic and C. Ahn, Nat. Phys. **10**, 892 (2014).
- [11] R. Peng *et al.*, Nat. Commun. **5**, 5044 (2014).
- [12] R. Peng *et al.*, Phys. Rev. Lett. **112** (2014).
- [13] F. Li *et al.*, Phys. Rev. B **91**, 220503 (2015).
- [14] Y. Miyata *et al.*, Nat. Mater. **14**, 775 (2015).
- [15] C. J. Tang *et al.*, arXiv: 1508.06368 (2015).
- [16] J. J. Lee *et al.*, Nature **515**, 245 (2014).
- [17] D. H. Lee, arXiv: 1508.02461.
- [18] J. Bang *et al.*, Phys. Rev. B **87**, 220503 (2013).
- [19] Z. Wang *et al.*, Proc. Natl. Acad. Sci. U.S.A. **111**, 3933 (2014).
- [20] A. F. Santander-Syro *et al.*, Nature **469**, 189 (2011).
- [21] T. Sakudo and H. Unoki, Phys. Rev. Lett. **26**, 851 (1971).
- [22] F. C. Hsu *et al.*, Proc. Natl. Acad. Sci. U.S.A. **105**, 14262 (2008).
- [23] B. C. Russell and M. R. Castell, Phys. Rev. B **77** (2008).

- [24] J. A. Enterkin *et al.*, Nat. Mater. **9**, 245 (2010).
- [25] See Supplementary Material at [for a description of further details related to sample preparation methods, measurement methods and more STM topography images.](#)
- [26] G. Herranz *et al.*, Nat. Commun. **6**, 6028 (2015).
- [27] J. Bardeen *et al.*, Phys. Rev. **108**, 1175 (1957).
- [28] J. M. Kosterlitz and D. J. Thouless, J. Phys. C: Solid State Phys. **6**, 1181 (1973).
- [29] N. Reyren *et al.*, Science **317**, 1196 (2007).
- [30] B. I. Halperin and D. R. Nelson, J. Low. Tem. Phys. **36**, 599 (1979).
- [31] W. Zhang *et al.*, Phys. Rev. B **89**, 060506 (2014).
- [32] J. P. Hu and H. Ding, Sci. Rep. **2**, 381 (2012).
- [33] Y. Cao *et al.*, J. Chem. Phys. **137**, 044701 (2012).
- [34] A. Lopez *et al.*, Surf Sci. **494**, L811 (2001).

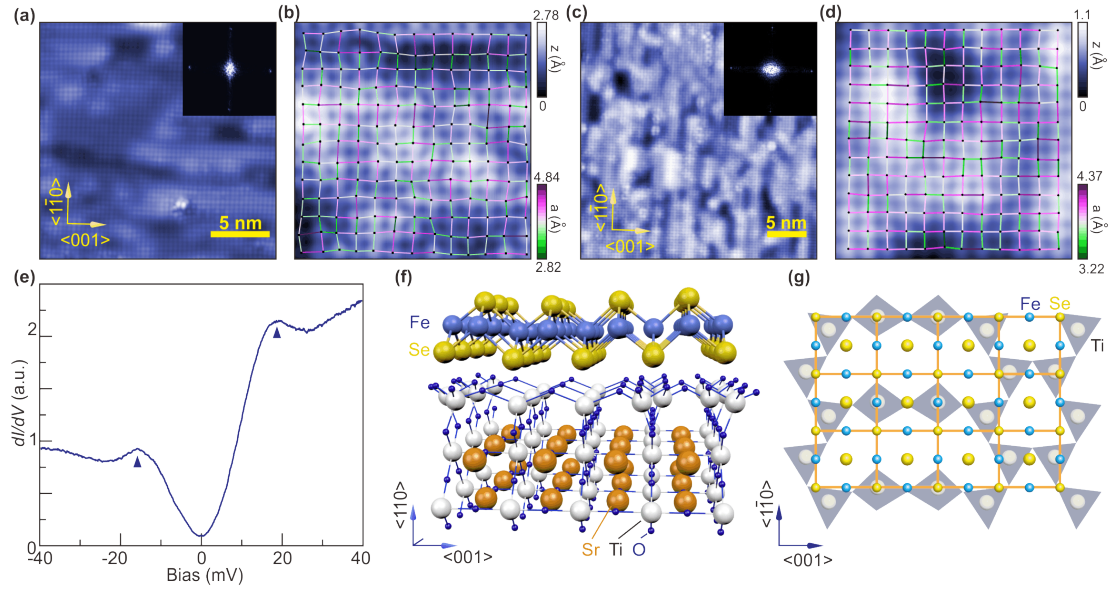


Fig. 1 (color online) (a)-(d) STM topography of 1-UC FeSe films on Nb-STO(110) substrate ((a) $V=200$ mV, $I=100$ pA and (b) $V=30$ mV, $I=300$ pA) and on insulating STO(110) substrate ((c) $V=100$ mV, $I=50$ pA and (d) $V=300$ mV, $I=200$ pA). The insets in (a) and (c) are the corresponding fast Fourier transform images ($6.0 \text{ nm}^{-1} \times 6.0 \text{ nm}^{-1}$). In (b) and (d), local maxima (black dots) are used as an approximate position of Se atoms, the distance between adjacent atoms are manifested by the colored segments. (e) Typical dI/dV curves taken on FeSe films ($V = 30$ mV, $I = 200$ pA). The triangles show the positions of coherent peaks. (f) Sketch of 1-UC FeSe epitaxially grown on STO(110)- (4×1) . (g) Schematic of the coincidence site lattice in 1-UC FeSe on STO(110)- (4×1) .

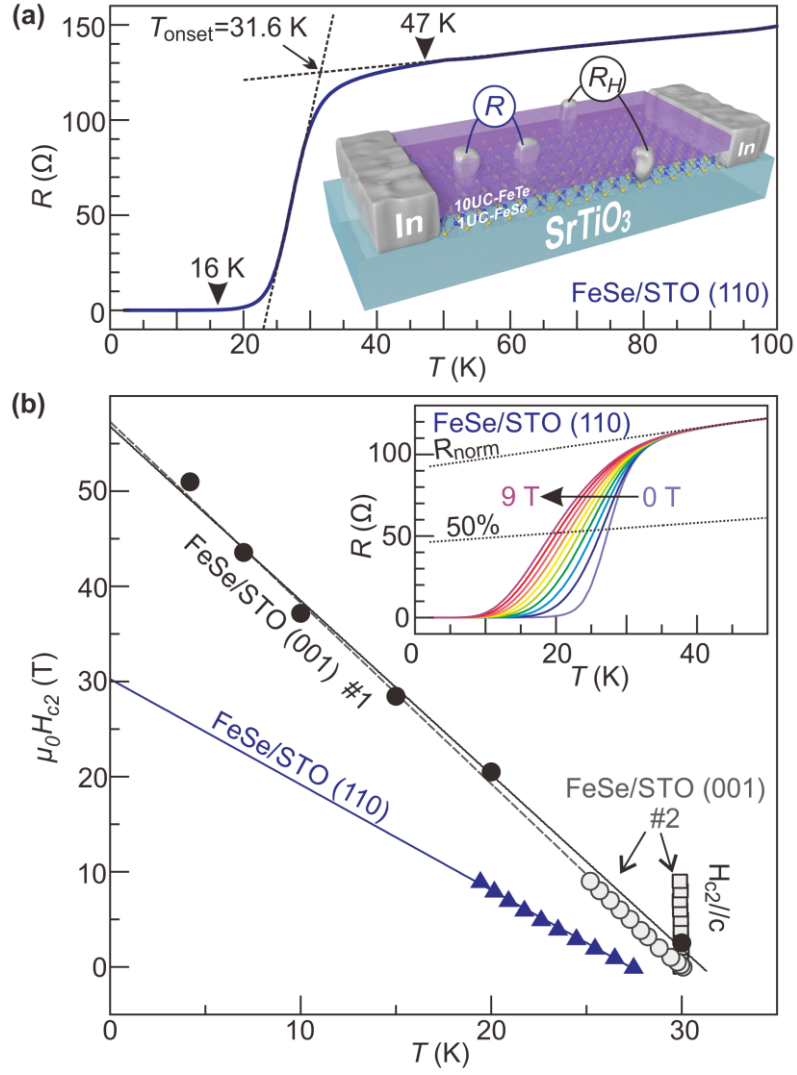


FIG. 2 (color online) (a) Resistance of the 10UC-FeTe/1UC-FeSe/STO(110) system as a function of temperature. Inset shows the schematic for measuring the longitudinal and the Hall resistance. (b) Upper critical field as a function of temperature for FeSe/STO(110) and FeSe/STO(001). Inset shows $R(T)$ of FeSe/STO(110) at magnetic fields from 0 to 9 T with increment of 1 T. Here the normal state resistance is normalized to the resistance in the temperature range of 40-50 K. Filled circles are obtained from a sample measured in a pulsed magnetic field reported in ref. [6]. Empty circles and squares are from a second FeSe/STO(001) sample where a static magnetic field is applied either perpendicular or parallel to the interface. Straight lines are extrapolations of the linear fittings.

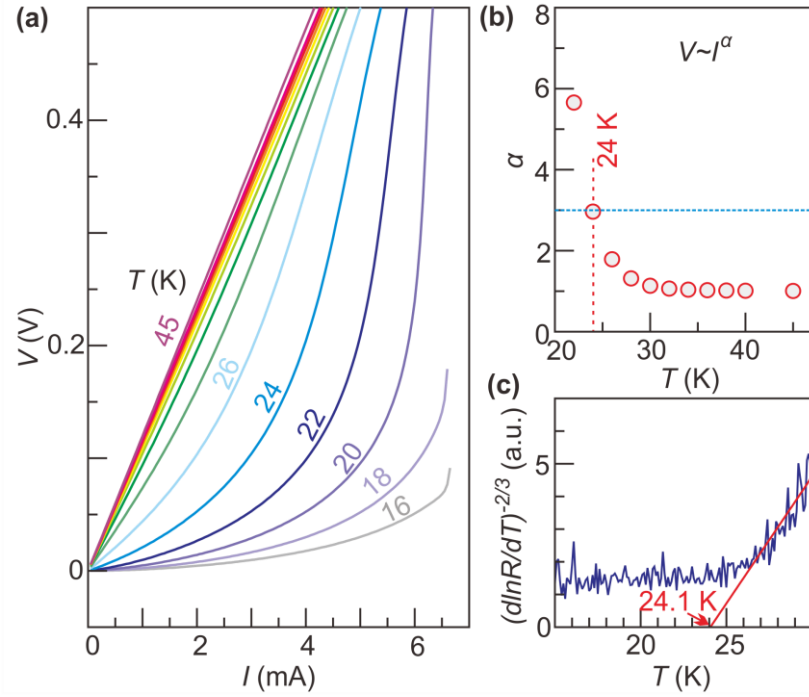


FIG.3 (color online) (a) Voltage as a function of current at different temperatures. Except for the data at 45 K, other curves are obtained from 40 to 16 K with a step of 2 K. (b) Temperature dependence of the power law exponent α determined from $V \sim I^\alpha$. The exponents are extracted from fittings to the data presented in (a). (c) R-T dependence on a $[d\ln(R)/dT]^{-2/3}$ scale. The Halperin-Nelson formula $R(T) = R \exp[-b(T/T_{BKT}-1)^{-1/2}]$ states that $[d\ln(R)/dT]^{-2/3}$ has a linear dependence on T above T_{BKT} . The red straight line is such a fit that extrapolates to zero at a BKT temperature of 24.1 K.

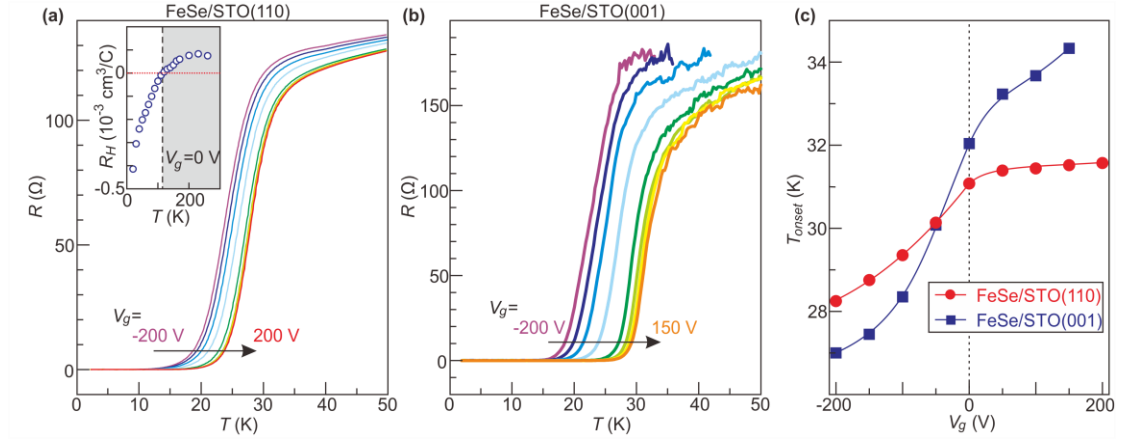


FIG. 4 (color online) (a) and (b) $R(T)$ curves at various gate voltages measured on 10UC-FeTe/1UC-FeSe/STO(110) and a 10UC-FeTe/1UC-FeSe/STO(100) systems, respectively. Inset to (a) displays the Hall coefficient as a function of temperature for the FeSe/STO(110) system. Data in (b) is taken from ref. [31]. (c) T_{onset} as a function of gate voltage for the FeSe/STO(110) and FeSe/STO(001) systems.

Supplemental Material for:

Observation of interface induced high temperature superconductivity in single unit-cell FeSe films on SrTiO₃(110)

Guanyu Zhou, Ding Zhang, Chong Liu, Chenjia Tang, Xiaoxiao Wang, Zheng Li, Canli Song, Shuaihua Ji, Ke He, Lili Wang, Xucun Ma and Qi-Kun Xue

The supplementary information includes:

1, Materials and Methods

2, Fig. S1, S2

Materials and Methods

The Nb-STO(110) substrates were heated to 1100 °C for 30 minutes in UHV chamber. After this treatment, the surface shows uniform (4×1) reconstruction (Fig. S1). The insulating STO(110) substrates were pretreated by chemical etching in a 10% -HCl solution followed by thermal annealing in a tube furnace at 1080 °C for 3 hours, and then loaded into the UHV chamber and degassed at 600 °C for 30 minutes.

The growth of single unit-cell FeSe film on the above-mentioned Nb-STO and insulating (110) substrates was carried out in ultra-high vacuum STM-MBE systems. Stoichiometric FeSe was obtained by co-evaporating Fe (99.995%) and Se (99.9999%) with a flux ratio of 1:10 at a substrate temperature of 400 °C and post-annealing at a temperature up to 500 °C for several hours. The growth rate was approximately 0.2 UC/min.

In all STM/STS measurements, a polycrystalline PtIr tip was used. The STS was acquired at 4.6 K by using lock-in technique with a bias modulation of 0.4 mV at 837 Hz and set point of 30 mV, 200 pA.

For *ex-situ* transport measurement, FeTe protection layers were grown on FeSe films by co-evaporating Fe (99.995%) and Te (99.9999%) with a flux ratio of ~ 1:4 on the FeSe films at 320 °C. The samples were then taken out from UHV chamber and electrically contacted by

cold-pressed indium. The resistance was measured by the standard lock-in technique (Stanford Research 830, $I_{ac}=1 \mu A$, 13Hz). DC current-voltage characteristics were obtained by driving the current from the source to the drain and measuring four-terminal longitudinal voltage with a pre-amplifier (Keithley 2400 as the current source, Stanford Research 560 as the amplifier). Cryogenic temperature and high magnetic field were realized in a commercial physical property measurement system (PPMS, Quantum Design).

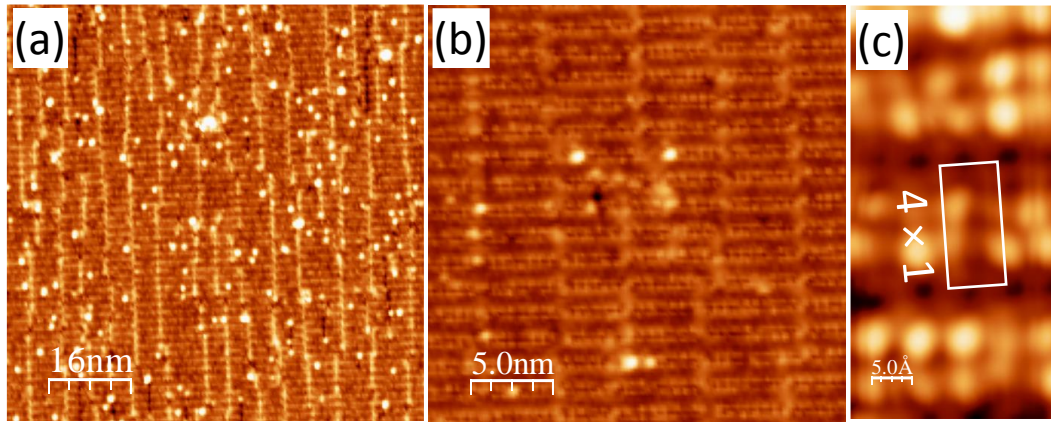


FIG. S1 (color online) (a)-(b) STM topography of Nb-STO(110) substrate before FeSe deposition ((a)-(b) $V=1 V$, $I=50 pA$ and (c) $V=500 mV$, $I=100 pA$). The rectangle in (c) shows a unit of (4×1) reconstruction.

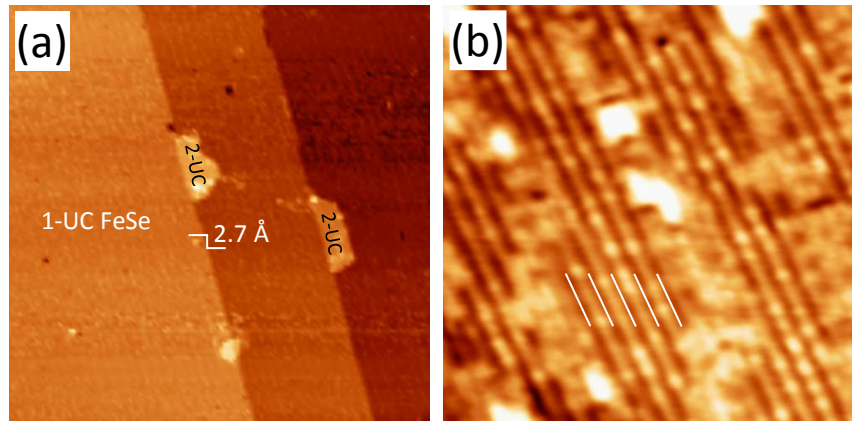


FIG. S2 (color online) STM topography of 1-UC FeSe films on insulating STO(110) substrate ((a) $V=1V$, $I=100 pA$, $250 nm \times 250 nm$ and (b) $V=600 mV$, $I=100 pA$, $50 nm \times 50 nm$). Short lines in (b) are equidistant with a spacing of 2.4 nm. This value corresponds nicely to the (6×1) reconstruction of TiO_4 layer on $SrTiO_4^{4+}$ surface.